Atmos. Chem. Phys. Discuss., 11, 1219–1264, 2011
www.atmos-chem-phys-discuss.net/11/1219/2011/
doi:10.5194/acpd-11-1219-2011

Atmospheric Chemistry and Physics Discussions

Quantification of aerosol chemical composition using continuous single particle measurements

C.-H. Jeong[1], M. L. McGuire[1], K. J. Godri[2], J. G. Slowik[1], P. J. G. Rehbein[1], and G. J. Evans[1]

[1]Southern Ontario Centre for Atmospheric Aerosol Research, University of Toronto, 200 College Street, Toronto, Ontario, M5S 3E5, Canada
[2]Division of Environmental Health & Risk Management, School of Geography, Earth & Environmental Sciences, University of Birmingham, Edgbaston, Birmingham, B15 2TT, UK

Received: 5 November 2010 – Accepted: 22 December 2010 – Published: 17 January 2011

Correspondence to: G. J. Evans (greg.evans@utoronto.ca)

Published by Copernicus Publications on behalf of the European Geosciences Union.

Abstract

Mass concentrations of particulate matter (PM) chemical components were determined from data for 0.3 to 3.0 µm particles measured by an Aerosol Time-of-Flight Mass Spectrometer (ATOFMS) data at an urban and rural site. Hourly-averaged concentrations of nitrate, sulphate, ammonium, organic carbon, and elemental carbon, estimated based on scaled ATOFMS peak intensities of corresponding ion marker species, were compared with collocated chemical composition measurements by an Aerosol Mass Spectrometer (AMS), a Gas-Particle Ion Chromatograph (GPIC), and a Sunset Lab field OCEC analyzer. The highest correlation was found for nitrate, with correlation coefficients (Pearson *r*) of 0.89 and 0.85 at the urban and rural sites, respectively. ATOFMS mass calibration factors, determined for the urban site, were used to calculate mass concentrations of the major PM chemical components at the rural site. Mass reconstruction using this ATOFMS based composition data agreed very well with the total PM mass measured at the rural site. Size distributions of the ten main types of particles were resolved for the rural site and the mass composition of each particle type was determined in terms of sulphate, nitrate, ammonium, organic carbon and elemental carbon. This is the first study to estimate hourly mass concentrations of individual aerosol components and the mass composition of individual particle-types based on ATOFMS single particle measurements.

1 Introduction

Numerous epidemiological studies have revealed significant associations between adverse cardiorespiratory health and exposure to atmospheric particulate matter (PM) with an aerodynamic diameter less than 2.5 µm ($PM_{2.5}$) (e.g., Dockery et al., 1993; Burnett et al., 1995; Schwartz and Dockery, 1996; Janssen et al., 2003). Deviations between the strength of the association identified by these studies reflect the use of PM mass concentration which is insensitive to heterogeneities in physical and chemical PM characteristics (Kunzli et al., 2006). Toxicology studies have documented that

ACPD
11, 1219–1264, 2011

specific PM components contribute to the observed toxicity: catalytic transition metals (Stohs and Bagchi, 1995), surface adsorbed organics (polycyclic aromatic hydrocarbons and quinones) (Squadrito et al., 2001) and endotoxins (Thorne, 2000) are able to elicit oxidative stress in the lung via their direct or indirect ability to generate reactive oxygen species (Pourazar et al., 2005).

A real-time, single particle instrument, such as an Aerosol Time-of-Flight Mass Spectrometer (ATOFMS), can provide size resolved chemical information on ambient PM in real time. To characterize individual ambient particles, ATOFMS instruments have been deployed in several sites in the US, Greece, and Mexico (e.g., Shields et al., 2008; Dall'Osto and Harrison, 2006; Moffet et al., 2008). An aerosol Laser Ablation Mass Spectrometer (LAMS) was first deployed in Canada during the winter of 2000 (Tan et al., 2002). Quantification of chemically resolved composition in ambient particles obtained by ATOFMS measurements is problematic mostly due to particle size and shape dependent transmission efficiency, chemical composition dependent ionization efficiency, and variability in ion intensity for identical particles (Allen et al., 2000; Kane and Johnston, 2000; Reilly et al., 2000; Wenzel and Prather, 2004). The transmission bias was evaluated by comparing ATOFMS data with size segregated mass concentrations measured by a Micro-Orifice Uniform Deposit Impactor (MOUDI) (Allen et al., 2000; Bhave et al., 2002). Several studies have suggested procedures to scale ATOFMS measurements using collocated optical particle counters (Wenzel et al., 2003; Qin et al., 2006; Dall'Osto and Harrison, 2006). Qin et al. (2006) and Dall'Osto et al. (2006) corrected for transmission losses by scaling with an Aerodynamic Particle Sizer (APS) and the scaled values agreed with total $PM_{2.5}$ mass concentrations and 24-h sampled chemical species collected by a MOUDI. Spencer and Prather (2006) compared unscaled organic carbon (OC) and elemental carbon (EC) fractions estimated from ATOFMS ion intensities with OC and EC concentrations determined using semi-continuous thermo-optical measurements. These studies used time averaging of several hours or more. However, hourly to sub-hourly time-resolved chemical speciation is needed to characterize the rapid changes that can occur in $PM_{2.5}$ composition.

ACPD
11, 1219–1264, 2011

An ATOFMS was deployed in two winter/summer field campaigns conducted in downtown Toronto and Harrow, a metropolitan area and a rural area, respectively, in Southern Ontario, Canada. One of the objectives of these field campaigns was to compare the chemical components measured by the ATOFMS with collocated high time resolution measurements. In the study, the quantitative measurements of particulate nitrate, sulphate, ammonium, OC, and EC ion markers in single particle mass spectra were obtained by scaling peak intensities (relative peak area and absolute peak area) of the marker ions measured by the ATOFMS. An enhanced procedure was developed to scale the ATOFMS transmission using both a TSI 3321 APS and a TSI 3091 Fast Mobility Particle Sizer (FMPS). The quantitative chemical information estimated using ATOFMS ion intensity data was compared to collocated high-time resolution chemical species concentrations measured by an Aerodyne Aerosol Mass Spectrometer (AMS), a Dionex Gas-Particle Ion Chromatography (GPIC), and a Sunset Lab field thermal-optical OCEC (Sunset OCEC) analyzer in both the urban and rural locations.

Mass concentrations of major chemical species were estimated using the ATOFMS, based on linear correlation analysis between the scaled ATOFMS and measurements by the GPIC as well as the Sunset OCEC analyzer. Total $PM_{2.5}$ mass were reconstructed from the ATOFMS chemical species at the two sites and evaluated by comparison with measured $PM_{2.5}$ mass concentrations.

2 Experimental methods

2.1 Sampling sites and measurements

An ATOFMS (TSI 3800-100) was deployed in downtown Toronto, Ontario, Canada from 20 January 2007 to 5 February 2007 as a part of the Seasonal Particulate Observation in Regional Toronto (SPORT) campaign (Fig. 1). The Toronto site (43°39′32.40″ N, 79°23′43.44″ W), a roadside building at the Southern Ontario Centre for Atmospheric

ACPD
11, 1219–1264, 2011

Aerosol Research (SOCAAR) of the University of Toronto, is located at the intersection of high traffic local streets (~33 000 vehicles/weekday). Busy expressways were situated to the east (~3 km) and south (~2 km) of the monitoring site. The main sampling inlet of the SOCAAR laboratory was approximately 15 m from the road and 6 m above the ground level. The diameter of the insulated sampling inlet was ~10 cm and the length was ~8 m. During the SPORT campaigns, the ATOFMS was deployed with other collocated chemical speciation instruments; a GPIC and a Sunset OCEC analyzer.

The Border Air Quality and Meteorology Study (BAQS-Met 2007) was a summer intensive field study conducted in several locations across southern Ontario to investigate the influence of local and trans-boundary transported pollutants on local air quality. As part of the BAQS-Met 2007 an ATOFMS was deployed in a rural area in Harrow, Ontario, Canada (42°1′58.95″ N, 82°53′35.61″ W) ~340 km southwest of the Toronto site for the period 19 June to 11 July 2007 (Fig. 1). The Harrow site located near Lake Erie was influenced by local industrial sites including the Detroit-Windsor industrial area and long-range transported emissions from industrial areas in the Midwestern US. Measurements were performed in SOCAAR's mobile lab (MAPLE) using a stainless steel sampling tubing (2.5 cm in diameter, 5 m long). During the BAQS-Met 2007 campaign, a Time-of-Flight Aerodyne AMS was also simultaneously deployed. Comparisons were made between the ATOFMS quantitative measurements and corresponding chemical speciation data provided by the AMS and Sunset OCEC analyzer.

Basic instrumental descriptions of a TSI 3800 ATOFMS are presented in detail elsewhere (e.g., Gard et al., 1997). In brief, ambient particles (0.1 L/min) are drawn thorough an aerodynamic focusing lens (AFL, TSI AFL-100) to the ATOFMS sizing region. In this sizing region the aerosols are accelerated to their terminal velocities depending on their aerodynamic diameters which are then determined by measuring the transit time between two 50 mW Nd:YAG lasers (532 nm). Once the particles enter the mass spectrometer region, a UV laser (Nd:YAG 266 nm, ~10^8 W cm^{-2}) desorbs and ionizes the particles to produce positive and negative ions. These ions are accelerated and

ACPD
11, 1219–1264, 2011

detected by dual detecting plates, providing positive and negative ion mass spectra for each particle. Polystyrene latex sphere (PSL, 0.2–2.1 µm) and TSI metal solutions were used for particle size and mass spectra calibration.

Hourly averaged concentrations of sulphate, nitrate, ammonium, and organics measured by the AMS were compared to the corresponding PM speciation concentrations measured by the ATOFMS. The AMS collection efficiencies (CE) were determined from the AMS light scattering module at Harrow (Quinn et al., 2006). The AMS data was corrected for the CE, varying between 0.5 and 1. The transmission particle size range of the AMS was less than 1 µm, representing PM_1 chemical component measurements, with nearly 100% transmission efficiency for particles between 0.07–0.50 µm (Jayne et al., 2000). A detailed description of an AMS is provided elsewhere (Jayne et al., 2000; Jimenez et al., 2003).

The GPIC measured $PM_{2.5}$ chemical speciation concentrations of both water soluble inorganic gaseous and ambient particles every 15 min, while the semi-continuous Sunset Lab field OCEC analyzer determined $PM_{2.5}$ OC and EC using the thermal-optical transmission (TOT) method with 2 h time resolution. Detailed descriptions of the GPIC and Sunset OCEC analyzer can be found elsewhere (Godri et al., 2009; Jeong et al., 2004). Hourly $PM_{2.5}$ data measured by a Tapered Element Oscillating Microbalance (TEOM) were obtained from the Toronto downtown monitoring site operated by the Ontario Ministry of the Environment, approximately 900 m northeast of the SOCAAR site. Since the heated inlet of the TEOM was operated at 40 °C, a negative artifact due to the loss of ammonium nitrate and semivolatile organics was expected in the TEOM $PM_{2.5}$ mass data. During the BAQS-Met campaign, continuous $PM_{2.5}$ mass concentrations were measured by a TSI 8520 DustTrak monitor and a Met One instrument 1020 Beta Attenuation Monitor (BAM) deployed by Environment Canada.

ACPD
11, 1219–1264, 2011

2.2 Data analysis

During the SPORT and the BAQS-Met campaigns, 1 806 910 and 183 410 particles were sized, respectively, and both size and positive/negative mass spectra data (hit particles) were collected for 588 570 and 66 920 ambient particles. The ion intensity for each mass to charge (*m/z*) within a particle mass spectrum was expressed as arbitrary units (AU), a measure of the number of ions of this *m/z* detected. All individual particle mass spectra were converted into a peak list using TSI MS-Analyze software with the following detection limit criteria: a peak had to contain at least 20 AU above the baseline, have at least 20 squared AU of area, and represent more than 0.1% of the total AU detected for the particle.

Mass to charge values within the positive and negative spectra were selected to estimate quantitative concentrations of the major chemical components in single particle mass spectra. The best *m/z* candidates for the major components were determined by comparing hourly particle counts from *m/z* −100 to +100 with relevant chemical concentrations obtained by the AMS and Sunset OCEC analyzer. A short list of ATOFMS *m/z* values were initially selected as candidate markers based on their strong correlation with chemical composition measured by the collocated instruments. The final ATOFMS *m/z* markers selected for sulphate, nitrate, ammonium, OC, and EC were *m/z* −97 [HSO_4^-], −62 [NO_3^-], +18 [NH_3^+], +43 [$C_3H_7^+$], and +36 [C_3^+]; the corresponding mass to charge peaks were integrated over ±0.4 Daltons. It should be noted that the use of multiple ions for a compound was also explored, (e.g., using the sum of *m/z* −97 [HSO_4^-] and −80 [SO_3^-] for sulphate). However, there was no improvement in the correlation between the ATOFMS ions peaks and the other collocated measurements. Hence a single *m/z* was selected as the marker for each aerosol component.

The particle detection efficiency of the ATOFMS depends on the ability of the instrument to transport particles to the ablation region of the instrument (the transmission efficiency) and the capacity of the particle to then absorb ablation laser photons in order to produce a measurable mass spectrum (the hit efficiency). Thus the detection efficiency depends on particle size, shape and composition (Allen et al.,

ACPD
11, 1219–1264, 2011

2000; Kane and Johnston, 2000). The lower transmission efficiencies of smaller sizes in the ATOFMS creates a bias towards particles of a given size range. In this work the number concentrations of particles hit by the ATOFMS for twelve size bins between 0.2 µm and 3.0 µm were scaled by the particle number concentrations simultaneously measured by an APS and an FMPS to correct for the detection efficiency. The APS measured the size distribution of particles from 0.5 µm to 20 µm in aerodynamic diameter with 1 min resolution. The APS also detected particles in the range of 0.3 µm to 0.5 µm using a light scattering mode. However, these light scattering data were not used due to the associated high uncertainty (Peters and Leith, 2003). Instead, particle number size distributions in the 0.1 µm to 0.5 µm range measured by the FMPS were selected for the ATOFMS count correction. The FMPS provided particle size distributions from 0.06 µm to 0.56 µm (electronic mobility diameter) with 1 s time resolution. The FMPS has been described in detail elsewhere (Jeong and Evans, 2009). We should note that calibrations with standard PSL particles of known size indicated that the FMPS underestimates the size of particles larger than 0.1 µm. Thus corrections factors were developed and applied based on these PSL particles. Application of this size correction was validated by comparing the size distributions for ambient particles measured by the FMPS and a TSI Scanning Mobility Particle Sizer (SMPS, TSI 3936).

Since there is a difference between aerodynamic and the electrical mobility diameter determined by the FMPS, particle diameters obtained by the FMPS were converted to aerodynamic diameter to allow a proper comparison. The conversion given by Sioutas et al. (1999) and Hinds (1982) was used:

$$d_a = d_m \sqrt{\frac{C_{c,d_m} \cdot \rho_{eff}}{C_{c,d_a} \cdot \chi \cdot \rho_0}} \quad (1)$$

where ρ_0 is the standard density ($1\,g\,cm^{-3}$), ρ_{eff} is the effective density, d_a is the aerodynamic diameter, d_m is the electrical mobility equivalent diameter, C_{c,d_m} is the Cunningham slip correction factor for the mobility equivalent diameter, C_{c,d_a} is the

ACPD
11, 1219–1264, 2011

Cunningham slip correction factor for the aerodynamic diameter, and χ is the dynamic shape factor. The effective diameter depends on both material density and shape of the particle. In this study, χ and ρ_{eff} were assumed to be 1 and 1.6 g cm^{-3}, respectively. These values were used in Eq. (1) to convert the FMPS mobility diameters in the size range of 0.09 µm to 0.39 µm, to aerodynamic diameters ranging from 0.11 µm to 0.50 µm. After transforming the FMPS scale from the mobility to the aerodynamic diameters, the APS and FMPS size distributions data were merged together in Fig. 2. Data for the similar particle diameter at ~0.5 µm were in reasonable agreement in general. However, in the overlapping diameter range (0.3 µm–0.5 µm) the APS concentration was lower than the FMPS data by a factor of ~2 at the both sites. This discrepancy might be due to the poorer counting efficiency of the TSI 3321 APS for the smallest particle size (<0.5 um) determined by only light scattering intensity information (Armendariz and Leith, 2002; Peters and Leith, 2003).

On average, the total number concentrations of particles in the size range of 0.01 µm–2.50 µm were 32 600 ± 800 cm^{-3} (mean ± standard error) and 16 000 ± 600 cm^{-3} for the winter time in Toronto and for the summer time in Harrow, respectively. This difference was evident for particles smaller than 0.1 µm and mostly due to the seasonal difference between the two sampling campaigns. The particle number concentrations in Toronto were ~34% lower than those in Harrow during the summer (Jeong et al., 2010). For particles in the 0.1 µm–0.5 µm range the number concentration in Harrow was higher than the average in Toronto by a factor of 1.2, whereas the number concentration of the largest mode particles (0.8 µm–2.5 µm) was higher in Toronto than the average in Harrow by a factor of two. In order to estimate size-specific scaling factors for the ATOFMS measurements, the number concentrations were converted into volume concentrations. A descriptive summary of particle volume concentrations measured by the FMPS and APS in Toronto and Harrow, respectively, is shown in Table 1. As expected, the average volume concentrations of particles in the size range of 0.1 µm–0.5 µm detected by the FMPS were distinctly higher than the average volume concentrations (0.3 µm–0.5 µm) measured by the APS.

ACPD
11, 1219–1264, 2011

A scaling factor (S) was defined as follows to correct for the ATOFMS' detection efficiency:

$$\text{For } d_a > 0.52\,\mu\text{m}, \qquad S_{d_{a,j}} = \frac{V_{j(\text{APS})}}{V_{j(\text{ATOFMS})}} \tag{2}$$

$$\text{For } d_a < 0.52\,\mu\text{m}, \qquad S_{d_a<0.52\mu\text{m}} = \frac{V_{0.1-0.5\mu\text{m(FMPS)}}}{V_{d_a<0.52\mu\text{m(ATOFMS)}}} \tag{3}$$

where $V_{j(\text{APS})}$ and $V_{j(\text{ATOFMS})}$ are the hourly total particle volume concentrations measured by the APS and ATOFMS measurements in the size bin (j), respectively; $V_{0.1-0.5\mu\text{m(FMPS)}}$ is the hourly total volume concentration of particles in the range from 0.1 µm to 0.5 µm (aerodynamic diameter) measured by the FMPS; and $V_{d_a<0.52\mu\text{m(ATOFMS)}}$ is the hourly total particle ($d_a < 0.52$ µm) volume concentration obtained by the ATOFMS. To calculate the total volume concentrations of particles ($d_a < 0.52$ µm) measured by the ATOFMS, an average diameter of 0.3 µm was assumed. Even though number concentrations in the smaller size range were available for both the FMPS and the ATOFMS, integrated values were used for the quantification approach due to the poor detection efficiencies of two instruments for this range. The midpoints of 11 size bins for the scaling factor with the APS were 0.56, 0.65, 0.75, 0.87, 1.00, 1.15, 1.33, 1.54, 1.78, 2.05, and 2.37 µm in this study.

We hypothesized that scaled ion intensities are linearly correlated with the volume concentrations of corresponding chemical components, and hence, relative peak areas (RPA) would be representative of the relative proportion of these chemical components in a single particle. Relative peak area was defined as the numbers of ions collected for a specific *m/z* divided by the total number of ions produced from the ionization of the particle. This was calculated as the peak area (PA) of the specific ion intensity divided by the total peak area of the positive or negative mass spectrum. Hourly fractional volumes ($v_{i,k}$, µm^3) of individual particles (i) for each ion marker (k) were estimated from:

ACPD
11, 1219–1264, 2011

$$v_{i,k} = \frac{\mathrm{RPA}_{i,k}}{2} \cdot \sum_i \frac{\pi}{6} d^3_{\mathrm{a}i,k} \quad (4)$$

where d_{ai} is the measured diameter (μm) of individual particle (i) for ion marker (k) and $\mathrm{RPA}_{i,k}$ is the ATOFMS relative peak area of *m/z*'s corresponding to chemical species, i.e., sulphate, nitrate, ammonium, OC, and EC. Implicit to this approach was the assumption that a particle was homogeneous or that it was fully ablated by the laser. It was further assumed that the ions observed in the positive and negative spectra contributed equally to the particle composition. Thus, the composition indicated by the RPA was scaled based on the volume of the particle.

Hourly scaled ATOFMS volume intensity (V_S, μm^3) of chemical species were estimated using hourly size specific scaling factors for the corresponding species as follows:

$$V_S = v_{i,k} \cdot S_{d_{ai,k}} \quad (5)$$

where $S_{d_{ai,k}}$ is the hourly scaling factor for each single particles corresponding to chemical species (k). Gross et al. (2000) reported that variations in relative peak areas of the ATOFMS ion intensity were smaller than absolute peak area variations for particles of identical composition. However, RPA of positive ions can be affected by particle compositions due to matrix effects (Reilly et al., 2000). For example, the ATOFMS efficiently ionizes potassium, as the ionization efficiency of potassium is significantly higher than any other measureable species. Thus the RPA of other *m/z* peaks in a positive spectrum may be affected by potassium.

In addition to using RPA, the scaled total ATOFMS peak area ($\mathrm{PA_s}$), as given in Eq. (6), was examined.

$$\mathrm{PA_s} = \sum_i \mathrm{PA}_{i,k} \cdot S_{d_{ai,k}} \quad (6)$$

The scaled ATOFMS peak area was also compared with high time resolution PM speciation data. Also implicit to this method was the assumption that particles were fully

ACPD
11, 1219–1264, 2011

ablated and thus the ion intensity for a given *m/z* was proportional to the total amount of the corresponding component within the particle.

2.3 Clustering analysis

In order to group the mass spectra obtained by the ATOFMS into a small number of classes, logarithmic scale ATOFMS data were imported in a MATLAB-based software toolkit known as YAADA (http://www.yaada.org). Once imported, a clustering method based on the Adaptive Resonance Theory Artificial Neural Network (ART-2a) algorithm (Song et al., 1999; Pharea et al., 2001) was applied with a vigilance factor of 0.3 and a learning factor of 0.05. The 33 particles clusters obtained by running ART-2a were manually re-grouped into 10 general particle-types based on their similarities in mass spectra, size distributions, and temporal trends. In this study, hourly size-specific scaling factors were applied to individual particles to estimate the average mass composition of each particle-type in terms of the major chemical components in Harrow.

3 Results and discussion

3.1 Detection, transmission and hit efficiency of the ATOFMS

The scaling factor is shown in Fig. 3 as a function of particle size during the SPORT campaign in downtown Toronto and the BAQS-Met study at a rural site in Harrow. This scaling factor represents the inverse of the detection efficiency and accounts for losses due to transmission and ionization or chemical detection. The largest scaling factor ($\sim 5.9 \times 10^3$ for Toronto, $\sim 1.5 \times 10^5$ for Harrow) was found for the smallest particle size bins (0.3–0.5 µm), corresponding to the lowest detection efficiency for particles smaller than 0.5 µm. This indicates that the scaling of the ATOFMS data was mostly due to its low detection efficiency for small particles. The detection efficiency in Toronto, on average, was higher than in Harrow by approximately an order of magnitude for particles

ACPD
11, 1219–1264, 2011

between 0.3 µm and 2.5 µm. The difference in the efficiency was attributed in part to degraded performance of the sizing lasers and the photomultiplier of the ATOFMS at Harrow. The transmission, and hence detection, efficiency improved dramatically when these were later replaced after the Harrow campaign.

The detection efficiency of ATOFMS should in theory be the product of particle transmission and particle hit efficiencies. The hit efficiency is defined as the number of particles for which both size and mass spectral data are obtained divided by the number of particles sized. The hit efficiency is a function of particle properties, i.e., size, shape, optical properties, and chemical composition as well as instrumental parameters, i.e., alignment and laser pulse energy (Kane and Johntson, 2000; Su et al., 2004). In order to evaluate instrumental parameters affecting the hit efficiency, ATOFMS data were obtained using various sizes of PSL particles generated by a TSI 3076 atomizer. As shown in Fig. 4, the highest hit efficiency (>50%) was observed for spherical PSL particles ranging from approximately 0.3 µm to 0.8 µm, while small (0.2 µm) and large (2.1 µm) PSL particles showed the lowest hit efficiencies. Moreover, the transmission efficiency of the smallest PSL was very poor due to weaker light scattering which influenced detection by the ATOFMS sizing module. Broader dispersion away from the ATOFMS ionization laser during transmission due to Brownian motion would contribute to the poor hit efficiency. In addition, the lower hit efficiency for the larger PSL particles (d_p=2.1 µm) would be likely due to the timing of the ablation laser not being optimized for larger particles. Decreased transmission efficiencies for small (<60 nm) and large (>400 nm) particles were identified (Liu et al., 2007). The lower detection efficiency for PSL particles larger than 1 µm was also observed by Kamphus et al. (2007) using a single particle mass spectrometer with an aerodynamic focusing lens.

With respect to the field measurements, the chemical biases of ATOFMS data were indirectly examined by comparing the hit efficiency in a given size bin. Figure 5 presents the average hit efficiency as a function of particle size during the two field campaigns. On average, the hit efficiency was 29 ± 14% in Toronto. During the BAQS-Met study in Harrow, average hit efficiency for total particles was 27 ± 20%. Note that the ATOFMS

ACPD
11, 1219–1264, 2011

laser pulse energy was kept at ~1 mJ/pulse during the two campaigns. Overall, the highest hit efficiency was observed for the 0.35 µm ambient particles with an average efficiency of 38 ± 11% in Toronto and 57 ± 14% in Harrow. In this study the chemical components of the smallest ambient particles detected by the ATOFMS were dominated by carbon cluster ions ($C^{\pm}_{12n}$), i.e., EC, a strong light absorber. In contrast to the higher hit efficiency of the smaller ambient particles, the particle hit efficiency for both sampling locations tended to be lower for particles larger than 1 µm. Further, the hit efficiency of ambient particles in the size range of 1.0–1.5 µm in Harrow (BAQS-Met) was lower than that in Toronto (SPORT), as presented in Fig. 5. This implies that there was a dependency of ATOFMS hit efficiency on particle physicochemical properties as well as the size dependent instrument performance as described previously. Since the monitoring site in Harrow was situated by agricultural areas, ambient particles larger than 1 µm likely contained a greater proportion of less absorbing or more reflective crustal materials, resulting in the lower hit efficiency. Dall'Osto et al. (2006) also reported that sea salt and crustal material particles detected by ATOFMS in a marine environment had very low hit efficiency (5–17%). The possible effects of particle hit efficiency on the ATOFMS performance reported in this study are discussed later in this paper.

3.2 Comparison between scaled ATOFMS and collocated measurements

Comparison analyses between scaled total particle volume obtained by the ATOFMS and collocated semi-continuous measurements of chemical composition in Toronto and Harrow are shown in Figs. 6 and 7. Table 2 provides a summary of the comparison between the quantitative data obtained using RPA and PA with the ATOFMS ion species peaks and the chemical species concentrations measured at the two sites. Unscaled total particle volume concentrations without inclusion of RPA or PA were also compared, as presented in Table 2.

In Toronto, fifteen minute average concentrations of nitrate, sulphate, and ammonium were measured by the GPIC, while two-hour-averaged OC and EC concentrations were

ACPD
11, 1219–1264, 2011

obtained by the Sunset OCEC analyzer. During the SPORT campaign in Toronto, the highest correlation between the ATOFMS and the GPIC was observed for nitrate followed by ammonia and sulphate, as shown in Table 2. Note that scaling based on transmission efficiency improved the correlation; correlation coefficients (Pearson r) between the hourly-averaged non-scaled ATOFMS relative peak areas for sulphate, nitrate, and ammonium and hourly corresponding concentrations from the GPIC in Toronto were only 0.21, 0.43, and 0.49 (vs. 0.79, 0.89, and 0.85 for ATOFMS scaled by both the APS and FMPS), respectively, indicating the importance of correcting for the ATOFMS detection efficiency. It should also be noted that scaling using the APS alone, rather than the APS and FMPS together, lowered the Pearson correlation coefficients for nitrate (r=0.70, $p < 0.05$), while there was little change in the correlations for sulphate and ammonium. The effectiveness of the APS in scaling only for sulphate and ammonium suggests that ammonium sulphate in Toronto was mostly in the large mode particles (>0.5 µm). Comparable correlation coefficients have been found when the GPIC has been compared to other high time resolution measurements at other urban and rural sites (Grover et al., 2006; Long and McClenny, 2006; Godri et al., 2009). Grover et al. (2006) found a correlation coefficient (Pearson r) of 0.82 between the GPIC and R&P 8400S sulphate instrument. For nitrate, the correlation coefficients between the GPIC and R&P 8400N nitrate measurements were 0.86 in Fresno (Grover et al., 2006), 0.92 in Rubidoux (Long and McClenny, 2006), and 0.86 in Toronto (Godri et al., 2009), all comparable with the scaled ATOFMS value of 0.89 found in this study.

Continuous sulphate, nitrate, and ammonium concentrations were obtained by the collocated AMS for the BAQS-Met study at the rural site in Harrow. The correlation analyses of the ATOFMS and AMS techniques showed that scaled ATOFMS nitrate ($r = 0.85$), sulphate ($r = 0.79$), and ammonium ($r = 0.70$) intensities were well correlated with the corresponding AMS measurements, similar to the SPORT campaign. Comparison of the ATOFMS and the AMS also showed better correlations using scaling based on the APS and FMPS rather than the APS alone. The stronger correlations, suggested that using both the FMPS and APS was a more precise way of scaling the

ACPD
11, 1219–1264, 2011

ATOFMS data. The correlation analysis showed that the scaled ATOFMS RPA method was a better way than using PA to quantify sulphate, nitrate, and ammonium.

The thermal-optical EC concentrations measured by the Sunset OCEC analyzer showed a lower correlation with the scaled ATOFMS ion signal at *m/z* +36 Daltons ($r = 0.41$ to 0.44); using the sum of the scaled ATOFMS EC-related ions, *m/z* +36, +48, and +60, instead did not improve the correlation. In general, potassium was often observed as a dominant peak in many positive spectra. As a result, RPA levels of other positive ions were often reduced by the presence of potassium, whereas this had less influence on PA. Conversely, PA based measurement of ion intensity was influenced by fluctuations due to heterogeneity within the profile of the ablation/ionization laser beam (Gross et al., 2000), whereas this was mostly normalized out by using RPA. It is noteworthy that the determination of thermal-optical OC and EC concentrations strongly rely on differences in temperature profiles and optical correction methods: thermal-optical transmission (TOT) and thermal-optical reflectance (TOR) (Chow et al., 2001, 2005). EC concentrations using the TOT protocol tend to be lower than the TOR method. During the SPORT campaign, Godri et al. (2009) reported that a comparison of 2-h Sunset OCEC measurements and 24-h filter-based analyses showed a weaker correlation for EC than for OC. Another probable explanation for the weak correlation of EC is the incomplete laser desorption and ionization of larger particles containing EC coated by OC and secondary inorganic species.

3.3 Effects of particle hit efficiency and instrumental bias

Although the scaled ATOFMS data were, in general, well correlated with other chemical composition measurements, a discrepancy occurred for sulphate and ammonium during elevated ammonium sulphate and nitrate days in Toronto (Fig. 6). This was evident through the temporal variability in the hit efficiency. Figure 8 presents the hit efficiency of particles smaller than 0.52 µm at the two sites. In Toronto the hit efficiency on 23 January was very low, dropping sharply from approximately 55% to 13% as the concentrations of sulphate, nitrate and ammonium increased (Fig. 6). It is postulated

ACPD
11, 1219–1264, 2011

that this reduced hit efficiency was due to coating of the particles with high albedo compounds such as ammonium sulphate and ammonium nitrate. Zhang et al. (2008) reported that the light scattering ability of aged soot particles coated with H_2SO_4 is significantly enhanced by a factor of ~10, as compared to freshly emitted soot particles, and internal mixing of aged soot particles with H_2SO_4 altered the morphology from fractal particulates to more spherical agglomerates during atmospheric aging. A decrease in the hit efficiency during episodic days was also observed on 25–26 June at the Harrow site (Fig. 8b). In order to examine the effect of particle mixing state on the ATOFMS hit efficiency, the correlation between the hit efficiency and the ratio of EC to the sum of sulphate, nitrate, ammonium, and OC was analyzed. Pearson correlation coefficients (r) were 0.50 ($p < 0.05$) at Toronto and 0.32 ($p < 0.05$) at Harrow. These positive correlations support the observation that lower hit efficiency seemed to be associated with lower EC compositions (higher fractions of coating constituents), indicating the influence of particle aging processes on the ATOFMS sensitivity. Hence, more long-range transport and regional background of aged particles became dominant during the episodic periods and contributed to the decrease in the ATOFMS hit efficiency.

3.4 Mass reconstruction

Linear regression parameters between the scaled ATOFMS RPA (V_s) and the GPIC/Sunset OCEC measurements for each chemical species in Toronto were calculated as presented in Table 3. These mass calibration factors were applied to determine the mass concentrations ($\mu g\,m^{-3}$) of corresponding $PM_{2.5}$ chemical components at both sites. Figure 9 describes the result when the estimated chemical components by the ATOFMS are plotted along with the total $PM_{2.5}$ mass concentrations measured by the TEOM and the DustTrak in Toronto and Harrow, respectively. In order to account for oxygen and hydrogen, organic matter (OM) was estimated from OC by applying a factor of 1.4 as suggested by Turpin and Lim (2001).

ACPD
11, 1219–1264, 2011

On average, nitrate was the largest contributor (36%) of the total $PM_{2.5}$ (sulphate + nitrate + ammonium + OM + EC) in the winter of Toronto, followed by OM (33%) and sulphate (18%). In Harrow, OM, sulphate, and nitrate accounted for approximately 41%, 23%, and 16% to the $PM_{2.5}$, respectively. As an agricultural area, the high contributions of OM and sulphate indicated the strong influence of secondary organic aerosols (SOA) from regional/trans-boundary sources.

The reconstructed mass (sulphate+nitrate+ammonium+OM+EC) from the scaled ATOFMS data correlated well with the total $PM_{2.5}$ mass ($r = 0.86$ for Toronto, $r = 0.87$ for Harrow). In Toronto, the regression between the total ATOFMS (y) and TEOM (x) measurements indicated a slope of 1.33 with an intercept of 3.81. Much of this difference was due to the loss of semi-volatile material in the TEOM monitor. The heated TEOM monitor volatilizes semi-volatile organics and ammonium nitrate especially in wintertime (Schwab et al., 2004, 2006). As shown in Fig. 9a, on the days of high ammonium nitrate, i.e., 23 January and 1 February 2007 the discrepancy tended to increase. Further, 68% of the $PM_{2.5}$ was on average present as organic mass or nitrate, components that could potentially volatilize in the TEOM. The negative bias in the TEOM were also previously reported during winter at this Toronto site, using reconstructed mass concentrations based on 24-h filter measurements or 2-h GPIC plus OCEC data (Godri et al., 2009).

For Harrow comparison of the reconstructed ATOFMS data (y) and the DustTrak $PM_{2.5}$ measurements (x) yielded a slope of 0.52 with an intercept of 4.62. As shown in Fig. 9b, the largest discrepancy was observed on 9–10 July. At the lower $PM_{2.5}$ concentration range ($<10\,\mu g\,m^{-3}$) the DustTrak $PM_{2.5}$ tended to be lower than the reconstructed ATOFMS, whereas the DustTrak data exceeded the ATOFMS data as the $PM_{2.5}$ mass increased at the higher concentration range above $10\,\mu g\,m^{-3}$. The reason for the discrepancy is still unknown but likely related to variation in the chemical composition. Excluding 9–10 July, the averages of the two measurements agreed almost perfectly, however, a recovery of 0.86 (i.e., slope with the intercept = 0) was obtained due to differences at low and high concentrations. This agreement must be emphasized

ACPD
11, 1219–1264, 2011

as the Harrow ATOFMS mass reconstruction was calculated based on calibration factors derived from the Toronto data, collected in winter not summer and at an urban instead of a rural site. Thus it appears that it may be possible to extend calibration factors from one site to another such that mass concentrations can be estimated from ATOFMS data even when no other co-located speciation instrumentation is available.

It is recommended that this approach to mass reconstruction, based on ATOFMS data, be further explored using data from additional sites, in order to better establish if or when calibration factors can in general be applied to multiple sites. In addition, more work is required in the estimation of the carbonaceous species. The correlation of the scaled ATOFMS and the Sunset OCEC measurements were poorer than the other three chemical species, sulphate, nitrate, and ammonium, thus the estimated OM and EC masses had higher uncertainties.

3.5 Scaling ATOFMS particle-types

The size-scaling and mass-calibration-factor methodology was also used in order to estimate the mass composition of different types of particles. The ATOFMS mass spectra measured in Harrow during the BAQS-Met campaign were analyzed using the ART-2a cluster algorithm. By merging similar clusters, a total of 33 clusters were reduced to 10 particle-types as shown in Table 4. The manually re-grouped particle-types accounted for 99% of the total hit particles. The contribution of the 10 particle-types to total detected particles and the most representative ions for each particle-type are presented in Table 4. A more detailed explanation for the particle-types is provided elsewhere (McGuire et al., 2011). Figure 10 exhibits the number fraction of these particle-types as a function of particle diameter. In this clustering analysis the number and size distributions of particles smaller than 0.5 µm were combined into one size bin. The 10 particle-types were scaled by the hourly size-specific scaling factors. Equation (5) was applied to each individual particle, of a given particle-type, to estimate hourly scaled volumetric intensities of the five major chemical components for that particle-type. In this quantification method the mass calibration factors in Table 3 were used to convert

ACPD
11, 1219–1264, 2011

the scaled volume intensities into mass concentrations ($\mu g\,m^{-3}$). The average mass concentration of the five chemical species and their contributions to the 10 particle-types are depicted in Fig. 11. It should be noted that, the mass concentrations and compositions in Fig. 11 are with respect to the five major chemical components. These five components represented the majority of the overall $PM_{2.5}$ mass, and thus presumably the majority of the mass for each particle-type. However, not all particles are detected by the ATOFMS, thus Fig. 11 does not necessarily represent a complete mass reconstruction.

Most of the particle-types contain at least some of all the components, indicating a high degree of internal mixing of these components. This is not surprising given that four of the five compounds were presumably secondary in nature, with EC representing the only primary compound. The particle-types differed mostly in terms of their relative ratios of sulphate, nitrate and ammonium, and organic to elemental carbon. The degree of external mixing of the minor components, not shown here, was greater.

The percent composition (Fig. 11) of the particle-types was also used to estimate their acidity ratio, the molar ratio of ammonium to nitrate + sulphate: $([NH^+]/18)/(2\times[SO_4^{2-}]/96+[NO_3^-]/62)$. On average, particle acidity analysis using the scaled mass concentrations showed that more than half (61%) of total particle mass concentration in Harrow were neutralized or slightly acidic with an acidity ratio of 0.75 ± 0.29 (mean ± standard deviation). The acidity ratios were generally within the expected range of 0.5 to 1.0, providing a further measure of the accuracy of the composition estimated for these particles. However, acidity ratios above 1.0 were found for some particle types, suggesting that errors remained in the estimation of some of the associated components. Thus the trends in the acidity ratios rather than their absolute values were used to compare the acidity of the particle-types.

The OC-S was the largest contributor (30%) to the total mass concentration measured by the ATOFMS, followed by the OC-S-N (29%). In addition, these two particle-types explained the majority (54–63%) of the sulphate, nitrate, ammonium, and OC in Harrow (Table 5). The OC-S particles were composed of similar amounts of organic

ACPD
11, 1219–1264, 2011

and inorganic components, with sulphate and ammonium making up most of the inorganic mass. This corresponded to the strong sulphate (*m/z* −97) and ammonium (*m/z* 18) in the mass spectra of the OC-S particles peaks, with the presence of high *m/z* organic peaks. The OC-S-N particles had similar composition but with more nitrate. Their spectra contained strong organic fragment peaks (i.e., *m/z* 27 and 43) mixed with loadings of organic nitrogen compounds (*m/z* −26 [CN^-] and −42 [CNO^-]).

The acidity ratio for the OC-S-N particles was 0.91 while that for the OC-S particles was 1.42, indicating that the OC-S-N particles where more acidic than the OC-S particles, consistent with the presence of more nitrate. While the OC-S-N types were observed through the whole campaign, the OC-S particles were mostly detected during the later period of the campaign (5 July to 6 July), when more organic mass was present (Fig. 7).

The OC-rich particle-type contained a large amount of organic mass and contributed ∼16% of the total mass, measured by the ATOFMS at the Harrow site. The OC-rich particles were similar in composition to the OC-S particles except that their mass spectra contained a much larger K^+ peak. The presence of potassium in particle mass spectra has previously been found to be a good marker of biomass burning (Bein et al., 2008). Further these particles had a relatively small mode in their size distribution at ∼0.45 µm, suggesting that this potassium did not originate from soil road dust. The OC-rich particles had an acidity ratio of 0.87and thus were more acidic than the other OC particle-types.

The EC-OC particles contained much (42%) of the elemental carbon and had a high ratio of elemental to organic carbon (Table 5). The spectra of the EC-OC particles had clear EC peaks at *m/z* ±12 and ±36 and organic fragments with *m/z* −97 ion peaks. This type contributed 11% of the total mass detected by the ATOFMS. The EC-OC was the most abundant particle-type on a particle number basis.

ACPD
11, 1219–1264, 2011

The amine and fireworks particle-type were only observed on certain days. For example, a large number of fireworks particles were observed on 5 July, the day after the 4th of July celebration. The fireworks particles contained large amounts of nitrate, possibly as residue from the KNO_3 used in the gun powder. The mass spectra of fireworks particle-type was characterized by strong Mg^+, K^+, and nitrate with the presence of *m/z* 88[Sr^+], *m/z* 154[$BaOH^+$], and *m/z* −163[$K(NO_3)_2^-$]. Although the mass contribution of the fireworks particle type was negligible, this type had a very low acidity ratio of 0.2. This low ratio was consistent with the nitrate being associated with alkaline earth compounds (e.g., KNO_3) rather than ammonium and thus was likely not indicative of high acidity. The amine type contained a high abundance of organic matter and more nitrate than sulphate. The presence of amine was identified by peaks at *m/z* 59 [C_3H_9N]; these particles also had OC fragments and low negative ion peaks in their mass spectra. The amine particles accounted for 7% of the total mass measured by the ATOFMS were only observed during periods of high relative humidity (Rehbein et al., 2010).

The EC (I) and EC (II) particles contained high proportions of elemental carbon. The mass spectra of the EC (I) particles had clear $C_{12n}^{\pm}$ fragment peaks (e.g., *m/z* ±12, ±24, ±36) and a strong Na^+ peak at *m/z* 23 while those for the EC (II) type also had higher sulphate and nitrate intensities with the $C_{12n}^{\pm}$ fragment peaks. The size distribution of the EC (I) type exhibited the small mode at ∼0.25 µm. The small size and low sulphate to elemental carbon suggested that these particle types were associated with fresh emissions from fossil combustion processes. The EC (I) type was observed in other ATOFMS studies at different locations (Dall'Osto et al., 2005; Moffet et al., 2008). The larger size mode (0.84 µm) of the EC (II) type and the presences of sulphate and nitrate peaks suggested that this particle-type was associated with aging. The EC (II) particles may have been a more processed version of the EC (I) particles.

Two dust-related types (Dust, Dust-Na) were found with relatively larger modes (>0.8 µm) in their size distributions with the common presence of *m/z* −16 and −17 as well as peaks at *m/z* −46 and 23. The Dust type was characterized by strong crustal element peaks at *m/z* 24[Mg^+], 27[Al^+], 39[K^+], 56[CaO^+] mixed with more organic

ACPD
11, 1219–1264, 2011

fragments, whereas the Dust-Na type was more clearly associated with Na^+ and fragments (e.g., 131[$NaNO_2NO_3^-$], 147[$Na(NO_3)_2^-$]) of sodium nitrate. Of the five compounds quantified, nitrate was the most important contributor to the mass of the dust related particle-types (Fig. 11b); other compounds not quantified from the ATOFMS data, such as mineral oxides, likely also contributed. The low content of ammonium indicated an internal mixture of nitrate and mineral dust components, possibly $CaNO_3$ and $NaNO_3$. The reactions of HNO_3 with NaCl or $CaCO_3$ are well-known depletion mechanisms of HNO_3 in the atmosphere (Myhre et al., 2006). The dust group particles were mostly larger in size; the Dust-Na cluster showed the largest size distribution with a mode of 1.8 µm.

To the best of our knowledge, this is first time that the mass composition of individual particle-types has been estimated based on real time single particle data. It should be emphasized that the reported compositions are estimates and the methodology still requires refinement. Specifically, implicit in the approach was the assumption that compounds exhibited similar sensitivities within different particle-types. This assumption needs to be further investigated.

4 Conclusions

Mass concentrations of $PM_{2.5}$ chemical components were determined from ATOFMS data collected at urban and rural sites during the SPORT and BAQS-Met field campaigns. In order to account for the temporal changes in the particle detection efficiency of the ATOFMS, the ATOFMS data were scaled using particle number concentrations measured simultaneously by an APS and FMPS. Hourly scaled volume concentrations of the five chemical species were estimated using the ATOFMS relative peak area (RPA) and these hourly size-specific scaling factors. This approach allowed sulphate, nitrate, ammonium, OC, and EC mass concentrations to be derived for the first time based on real-time single particle ATOFMS measurements. Sensitivity analysis was performed by comparing this approach to results obtained using peak area (PA)

ACPD
11, 1219–1264, 2011

instead (i.e., PA vs. RPA), as well as results obtained using only the APS for scaling (i.e., APS alone vs. APS + FMPS). This sensitivity analysis further validated the approach selected.

During the SPORT campaign in Toronto, nitrate ($r = 0.89$) showed the strongest correlation between the ATOFMS and parallel GPIC measurements. Good correlations were also observed for ammonia ($r = 0.85$) and sulphate ($r = 0.79$) in the urban area. The correlation analyses for the BAQS-Met study in Harrow also showed good correlations between the ATOFMS measurements and continuous nitrate ($r = 0.85$), sulphate ($r = 0.79$), and ammonium ($r = 0.70$) measured by a collocated AMS. Comparisons of OC and EC derived from the ATOFMS and a Sunset OCEC analyzer showed weaker correlations at the two sites.

Linear regression coefficients derived from the Toronto site were applied to both the Toronto and Harrow ATOFMS data in order to estimate the mass concentrations of the corresponding $PM_{2.5}$ chemical components. The reconstructed mass concentrations from the scaled ATOFMS were well correlated with continuous $PM_{2.5}$ measurements in the urban area (Toronto, $r = 0.86$, $p < 0.05$) and the rural area (Harrow, $r = 0.87$, $p < 0.05$). In the urban area nitrate was the largest contributor (~36%) to the total $PM_{2.5}$ in the winter, followed by OM (~33%) and sulphate (~18%). The summertime $PM_{2.5}$ in the rural area near the US border in Southern Ontario, was strongly influenced by regional/trans-boundary pollution resulting in a greater abundance of OM (~41%) and sulphate (~23%). The ATOFMS reconstructed mass for Harrow was based on regression parameters derived from Toronto data yet still agreed reasonably well with total mass measurements made at the Harrow site. Thus it appears that it may be possible to extend regression parameters from one site to another such that mass concentrations can be estimated from ATOFMS data even when no other co-located speciation instrumentation is available.

Ten major particle-types: OC-S, OC-S-N, OC-rich, EC-OC, Amines, Fireworks, EC (I), EC (II), Dust, Dust-Na were identified by applying the ART-2a clustering algorithm to ATOFMS ion mass spectra data collected from Harrow. The number and size

ACPD
11, 1219–1264, 2011

distributions of the 10 particle-types were scaled by the hourly size-specific scaling factors. The scaling significantly altered the size distributions and contributions of the particle-types. The quantification approach was also applied to scaled mass spectra of each particle-type so as to calculate the mass composition of each particle-type in terms of their major components. This approach provided new insight into the contribution made by different particle-types to the overall mass composition.

Acknowledgements. This work was supported by in part by the Ontario Ministry of the Environment and Environment Canada. Funding for SOCAAR was provided by the Canada Foundation for Innovation, the Ontario Innovation Trust and the Ontario Research Fund. The authors would like to thank Andrew Knox for OC and EC instrument operation at the Toronto site.

References

Allen, J. O., Fergenson, D. P., Gard, E. E., Hughes, L. S., Morrical, B. D., Kleeman, M. J., Gross, D. S., Galli, M. E., Prather, K. A., and Cass, G. R.: Particle detection efficiencies of aerosol time of flight mass spectrometers under ambient sampling conditions, Environ. Sci. Technol., 34, 211–217, 2000.

Armendariz, A. J. and Leith, D.: Concentration measurement and counting efficiency for the aerodynamic particle sizer 3320, J. Aerosol Sci., 33, 133–148, 2002.

Bein, K. J., Zhao, Y., Johnston, M. V., Evans, G. J., and Wexler A. S.: Extratropical waves transport boreal wildfire emissions and drive regional air quality dynamics, J. Geophys. Res., 113, D23213, doi:10.1029/2008JD010169, 2008.

Bhave, P. V., Allen, J. O., Morrical, B. D., Fergenson, D. P., Cass, G. R., and Prather, K. A.: A field-based approach for determining ATOFMS instrument sensitivities to ammonium and nitrate, Environ. Sci. Technol., 36, 4868–4879, 2002.

Burnett, R. T., Dales, R., Krewski, D., Vincent, R., Dann, T., and Brook, J. R.: Associations between ambient particulate sulfate and admissions to Ontario hospitals for cardiac and respiratory diseases, Am. J. Epidemiol., 172, 15–22, 1995.

Chow, J. C., Watson, J. G., Crow, D., Lowenthal, D. H., and Merrifield, T.: Comparison of IMPROVE and NIOSH carbon measurements, Aerosol Sci. Tech., 34, 23–34, 2001.

ACPD
11, 1219–1264, 2011

Chow, J. C., Watson, J. G., Chen, L.-W. A., Paredes-Miranda, G., Chang, M.-C. O., Trimble, D., Fung, K. K., Zhang, H., and Zhen Yu, J.: Refining temperature measures in thermal/optical carbon analysis, Atmos. Chem. Phys., 5, 2961–2972, doi:10.5194/acp-5-2961-2005, 2005.

Dall'Osto, M. and Harrison, R. M.: Chemical characterisation of single airborne particles in Athens (Greece) by ATOFMS, Atmos. Environ., 40, 7614–7631, 2006.

Dall'Osto, M., Harrison, R. M., Beddows, D. C. S., Freney, E. J., Heal, M. R., and Donovan, R. J.: Single-particle detection efficiencies of aerosol time-of-flight mass spectrometry during the North Atlantic marine boundary layer experiment, Environ. Sci. Technol., 40, 5029–5035, 2006.

Dockery, D. W., Pope, A., Xu, X., Spengler, J. D., Ware, J. H., Fay, M. E., Ferris, M. G., and Speizer, F. E.: An association between air pollution and mortality in six US cities, New Engl. J. Med., 329, 1753–175, 1993.

Gard, E., Mayer, J. E., Morrical, B. D., Dienes, T., Fergenson, D. P., and Prather, K. A.: Real-time analysis of individual atmospheric aerosol particles: design and performance of a portable ATOFMS, Anal. Chem., 69, 4083–4091, 1997.

Godri, K. J., Evans, G. J., Slowik, J., Knox, A., Abbatt, J., Brook, J., Dann, T., and Dabek-Zlotorzynska, E.: Evaluation and application of a semi-continuous chemical characterization system for water soluble inorganic $PM_{2.5}$ and associated precursor gases, Atmos. Meas. Tech., 2, 65–80, doi:10.5194/amt-2-65-2009, 2009.

Gross, D. S., Galli, M. E., Silva, P. J., and Prather, K. A.: Relative sensitivity factors for alkali metal and ammonium cations in single-particle aerosol time-of-flight mass spectra, Anal. Chem., 72, 416–422, 2000.

Grover, B. D., Eatough, N. L., Eatough, D. J., Chow, J. C., Watson, J. G., Ambs, J. L., Meyer, M. B., Hopke, P. K., Al-Horr, R., Later, D. W., and Wilson, W. E.: Measurement of both nonvolatile and semi-volatile fractions of fine particulate matter in Fresno, CA, Aerosol Sci. Tech., 40, 811–826, 2006.

Hinds, W. C.: Aerosol Technology: Properties, Behaviour, and Measurement of Airborne Particles, John Wiley, New York, 1982.

Janssen, N. A. H., Brunekreef, B., van Vliet, P., Aarts, F., Meliefste, K., Harssema, H., and Fischer, P.: The relationship between air pollution from heavy traffic and allergic sensitization, bronchial hyperresponsiveness, and respiratory symptoms in Dutch schoolchildren, Environ. Health Persp., 111, 1512–1518, 2003.

Jayne, J. T., Leard, D. C., Zhang, X. F., Davidovits, P., Smith, K. A., Kolb, C. E., and

ACPD
11, 1219–1264, 2011

Worsnop, D. R.: Development of an aerosol mass spectrometer for size and composition analysis of submicron particles, Aerosol Sci. Tech., 33, 49–70, 2000.
Jeong, C.-H. and Evans, G. J.: Inter-comparison of a fast mobility particle sizer and a scanning mobility particle sizer incorporating an ultrafine water-based condensation particle counter, Aerosol Sci. Tech., 43, 364–373, 2009.
Jeong, C.-H., Hopke, P. K., Kim, E., and Lee, D.-W.: The comparison between thermal-optical transmittance elemental carbon and Aethalometer black carbon measured at multiple monitoring sites, Atmos. Environ., 38, 5193–5204, 2004.
Jeong, C.-H., Evans, G. J., McGuire, M. L., Chang, R. Y.-W., Abbatt, J. P. D., Zeromskiene, K., Mozurkewich, M., Li, S.-M., and Leaitch, W. R.: Particle formation and growth at five rural and urban sites, Atmos. Chem. Phys., 10, 7979–7995, doi:10.5194/acp-10-7979-2010, 2010.
Jimenez, J.-L., Jayne, J. T., Shi, Q., Kolb, C. E., Worsnop, D. R., Yourshaw, I., Seinfeld, J. H., Flagan, R. C., Zhang, X. F., Smith, K. A., Morris, J. W., and Davidovits, P.: Ambient aerosol sampling using the Aerodyne Aerosol Mass Spectrometer, J. Geophys. Res., 108(D7), 8425, doi:10.1029/2001JD001213, 2003.
Kamphus, M., Ettner-Mahl, M., Brands, M., Curtius, J., Drewnick, F., and Borrmann, S.: Comparison of two aerodynamic lenses as an inlet for a single particle laser ablation mass spectrometer, Aerosol Sci. Tech., 42, 970–980, 2008.
Kane, D. B. and Johnston, M. V.: Size and composition biases on the detection of individual ultrafine particles by aerosol mass spectrometry, Environ. Sci. Technol., 34, 4887–4893, 2000.
Künzli, N., Mudway, I. S., Götschi, T., Shi, T., Kelly, F. J., Cook, S., Burney, P., Forsberg, B., Gauderman, J. W., Hazenkamp, M. E., Heinrich, J., Jarvis, D., Norbäck, D., Payo-Losa, F., Poli, A., Sunyer, J., and Borm, P. J. A.: Comparison of oxidative properties, light absorbance, and total and elemental mass concentration of ambient $PM_{2.5}$ collected at 20 European sites, Environ. Health Persp., 114, 684–690, 2006.
Liu, P. S. K., Deng, R., Smith, K. A., Williams, L. R., Jayne, J. T., Canagaratna, M. R., Moore, K., Onasch, T. B., Worsnop, D. R., and Deshler, T.: Transmission efficiency of an aerodynamic focusing lens system: comparison of model calculations and laboratory measurements for the aerodyne aerosol mass spectrometer, Aerosol Sci. Tech., 41, 721–733, 2007.
Long, R. W. and McClenny, W. A.: Laboratory and field evaluation of instrumentation for the semicontinuous determination of particulate nitrate (and other water-soluble particulate com-

ACPD
11, 1219–1264, 2011

ponents), J. Air Waste Manage., 56, 294–305, 2006.
McGuire, M. L., Jeong, C.-H., Slowik, J. G., Chang, R. Y.-W., Corbin, J. C., Lu, G., Mihele, C., Rehbein, P. J. G., Sills, D. M. L., Abbatt, J. P. D., Brook, J. R., and Evans, G. J.: Elucidating determinants of aerosol composition chemistry though particle-type based receptor modeling, Atmos. Chem. Phys. Disscuss., submitted, 2011.
Moffet, R. C., de Foy, B., Molina, L. T., Molina, M. J., and Prather, K. A.: Measurement of ambient aerosols in northern Mexico City by single particle mass spectrometry, Atmos. Chem. Phys., 8, 4499–4516, doi:10.5194/acp-8-4499-2008, 2008.
Myhre, G., Grini, A., and Metzger, S.: Modelling of nitrate and ammonium-containing aerosols in presence of sea salt, Atmos. Chem. Phys., 6, 4809–4821, doi:10.5194/acp-6-4809-2006, 2006.
Peters, T. M. and Leith, D.: Concentration measurement and counting efficiency of the aerodynamic particle sizer 3321, J. Aerosol Sci., 34, 627–634, 2003.
Phares, D. J., Rhoads, K. P., Wexler, A. S., Kane, D. B., and Johnston, M. V.: Application of the ART-2a algorithm to laser ablation aerosol mass spectrometry of particle standards, Anal. Chem., 73, 2338–2344, 2001
Pourazar, J., Mudway, I. S., Samet, J. M., Helleday, R., Blomberg, A., Wilson, S. J., Frew, A. J., Kelly, F. J., and Sandström, T.: Diesel exhaust activates redox-sensitive transcription factors and kinases in human airways, Am. J. Physiol.-Lung C., 289, L724–L730, 2005.
Qin, X., Bhave, P. V., and Prather, K. A.: Comparison of two methods for obtaining quantitative mass concentrations from aerosol time-of-flight mass spectrometry measurements, Anal. Chem., 78, 6169–6178, 2006.
Quinn, P. K., Bates, T. S., Coffman, D., Onasch, T. B., Worsnop, D., Baynard, T., de Gouw, J. A., Goldan, P. D., Kuster, W. C., Williams, E., Roberts, J. M., Lerner, B., Stohl, A., Pettersson, A., and Lovejoy, E. R.: Impacts of sources and aging on submicrometer aerosol properties in the marine boundary layer across the gulf of Maine, J. Geophys. Res. Atmos., 111, D23S36, doi:10.1029/2006JD007582, 2006.
Rehbein, P. J. G., Jeong, C.-H., McGuire, M. L., Yao, X., Corbin, J. C., and Evans, G. J.: Exploring the gas-to-particle partitioning of trimethylamine containing particles: the importance of fog and aerosol acidity, Environ. Sci. Technol., submitted, 2010.
Reilly, P. T. A., Lazar, A. C., Gieray, R. A., Whitten, W. B., and Ramsey, J. M.: The elucidation of charge-transfer-induced matrix effects in environmental aerosols via real-time aerosol mass spectral analysis of individual airborne particles, Aerosol Sci. Tech., 33, 135–152, 2000.

ACPD
11, 1219–1264, 2011

Schwab, J. J., Spicer, J., Demerjian, K. L., Ambs, J. L., and Felton, H. D.: Long-term field characterization of TEOM and modified TEOM samplers in urban and rural New York State locations, J. Air Waste Manage., 54, 1264–1280, 2004.
Schwab J. J., Felton, H. D., Rattigan, O. V., and Demergian, K. L.: New York State urban and rural measurements of continuous $PM_{2.5}$ mass by FDMS, TEOM, and BAM, J. Air Waste Manage., 56, 372–383, 2006.
Schwartz, J., Dockery, D. W., and Neas, L. M.: Is daily mortality associated specifically with fine particles?, J. Air Waste Manage., 46, 2–14, 1996.
Shields, L. G., Qin, X., Toner, S. M., and Prather, K. A.: Detection of ambient ultrafine aerosols by single particle techniques during the SOAR 2005 campaign, Aerosol Sci. Tech., 42, 674–684, 2008.
Sioutas, C., Abt, E., Wolfson, J. M., and Koutrakis, P.: Evaluation of the measurement performance of the Scanning Mobility Particle Sizer and Aerodynamic Particle Sizer, Aerosol Sci. Tech., 30, 84–92, 1999.
Song, X. H., Hopke. P. K., Fergenson, D. P., and Prather, K. A.: Classification of single particles analyzed by ATOFMS using an artificial neural network, ART-2a, Anal. Chem., 71, 860–865, 1999.
Spencer, M. T. and Prather, K. A.: Using ATOFMS to determine OC/EC mass fractions in particles, Aerosol Sci. Tech., 40, 585–594, 2006.
Squadrito, G. L., Cueto, R., Dellinger, B., and Pryor, W. A.: Quinoid redox cycling as a mechanism for sustained free radical generation by inhaled airborne particulate matter, Free Radical Bio. Med., 31, 1132–1138, 2001.
Stohs, S. J. and Bagchi, D.: Oxidative mechanisms in the toxicity of metal ions, Free Radical Bio. Med., 18, 321–336, 1995.
Su, Y. X., Sipin, M. F., Furutani, H., and Prather, K. A.: Development and characterization of an aerosol time-of-flight mass spectrometer with increased detection efficiency, Anal. Chem., 76, 712–719, 2004.
Tan, P. V., Evans, G. J., Tsai, J., Owega, S., Fila, M. S., Malpica, O., and Brook, J. R.: On-line analysis of urban particulate matter focusing on elevated wintertime aerosol concentrations, Environ. Sci. Technol., 36, 3512–3518, 2002.
Thorne, P. S.: Inhalation toxicology models of endo-toxin- and bioaerosol-induced inflammation, Toxicology, 152, 13–23, 2000.
Turpin, B. J. and Lim, H.-J.: Species contributions to $PM_{2.5}$ mass concentrations: revisiting

ACPD
11, 1219–1264, 2011

common assumptions for estimating organic mass, Aerosol Sci. Tech., 35, 602–610, 2001.
Wenzel, R. J. and Prather, K. A.: Improvements in ion signal reproducibility obtained using a homogeneous laser beam for on-line laser desorption/ionization of single particles, Rapid Commun. Mass Sp., 18, 1525–1533, 2004.
Wenzel, R. J., Liu, D.-Y., Edgerton, E. S., and Prather, K. A.: Aerosol time-of-flight mass spectrometry during the Atlanta Supersite Experiment: 2. scaling procedures, J. Geophy. Res., 108(D7), 8427, doi:10.1029/2001JD001562, 2003.
Yao, X., Shairsingh, K., Lam, P. H., and Evans, G. J.: Underestimation of sulfate concentration in $PM_{2.5}$ using a semi-continuous particle instrument based on ion chromatography, J. Environ. Monit., 11, 1292–1297, doi:10.1039/B819630C, 2009.
Zhang, R., Khalizov, A., Pagels, J., Zhang, D., Huaxin, X., and McMurry, P. H.: Variability in morphology, hygroscopicity and optical properties of soot aerosols during atmospheric processing, P. Natl. Acad. Sci. USA, 105, 10291–10296, 2008.

ACPD
11, 1219–1264, 2011

Table 1. Descriptive statistics for hourly averaged particle volumetric concentrations ($\mu m^3\,cm^{-3}$) measured by the FMPS and APS during the SPORT in Toronto and the BAQS-Met in Harrow.

		d_a^a (μm)	Mean	Median	StDev[b]	Min[c]	Max[d]	Lower Quartile	Upper Quartile	n^e
Toronto	FMPS	0.1–0.5	8.23	6.60	4.95	1.84	29.0	4.40	11.1	375
	APS	0.3–0.5	0.38	0.27	0.30	0.08	1.46	0.18	0.45	375
	APS	0.5–2.5	3.49	3.03	2.63	0.58	22.0	2.12	4.09	375
Harrow	FMPS	0.1–0.5	10.5	8.37	8.41	0.18	34.1	3.12	15.8	520
	APS	0.3–0.5	0.68	0.39	0.72	0.01	3.62	0.14	1.02	520
	APS	0.5–2.5	2.88	1.92	2.75	0.21	15.5	1.06	3.55	520

[a] Detection size range in an aerodynamic diameter.
[b] Standard deviation.
[c] Minimum.
[d] Maximum.
[e] Number of samples.

ACPD
11, 1219–1264, 2011

Table 2. Pearson correlation coefficients (r) between unscaled/scaled ATOFMS ion intensities and the hourly Sunset OCEC, GPIC (Toronto), and AMS (Harrow) measurements.

		Unscaled ATOFMS[a]			Scaled ATOFMS$^{c}_{A}$		Scaled ATOFMS$^{d}_{AF}$	
		Volume[b]	RPA	PA	RPA	PA	RPA	PA
Toronto	Sulphate (n[e] = 306)	0.12	0.21	0.33	0.80	0.78	0.79	0.60
	Nitrate (n = 304)	0.11	0.43	0.47	0.70	0.73	0.89	0.84
	Ammonium (n = 225)	0.48	0.49	0.59	0.85	0.87	0.85	0.74
	OC (n = 123)	0.40	0.50	0.66	0.21	0.25	0.45	0.55
	EC (n = 123)	0.34	0.32	0.54	0.23	0.29	0.44	0.53
Harrow	Sulphate (n = 426)	0.19	0.30	0.30	0.58	0.59	0.79	0.80
	Nitrate (n = 426)	0.57	0.59	0.65	0.70	0.65	0.85	0.70
	Ammonium (n = 426)	0.22	0.22	0.25	0.44	0.57	0.70	0.76
	OC (n = 227)	0.33	0.33	0.53	0.57	0.51	0.68	0.46
	EC (n = 227)	0.35	0.35	0.68	0.33	0.38	0.41	0.45

[a] Raw ATOFMS intensities for sulphate (m/z −97), nitrate (m/z −62), ammonium (m/z 18), OC (m/z 43), and EC (m/z 36).
[b] Total volume of particles corresponding ion intensities.
[c] ATOFMS$_A$ has corresponding ion intensities scaled by APS.
[d] ATOFMS$_{AF}$ has corresponding ion intensities scaled by APS and FMPS.
[e] Number of samples.

ACPD
11, 1219–1264, 2011

Table 3. Mass calibration factors derived from a correlation of the scaled ATOFMS volumetric intensity (V_s) and GPIC/Sunset OCEC measurements ($\mu g\,m^{-3}$) for $PM_{2.5}$ chemical components during the SPORT campaign. (Parameter values±standard errors.)*

	Slope (α)	Intercept (β)
[a]Sulphate (m/z −97)	$8.14 \times 10^{-5} \pm 3.19 \times 10^{-6}$*	$5.86 \times 10^{-1} \pm 6.21 \times 10^{-2}$
[a]Nitrate (m/z −62)	$2.28 \times 10^{-4} \pm 6.61 \times 10^{-6}$	$3.47 \times 10^{-1} \pm 1.29 \times 10^{-1}$
[a]Ammonium (m/z 18)	$6.47 \times 10^{-4} \pm 2.46 \times 10^{-5}$	$-2.55 \times 10^{-1} \pm 7.90 \times 10^{-2}$
[b]OC (m/z 43)	$3.83 \times 10^{-4} \pm 6.88 \times 10^{-5}$	$1.80 \times 10^{0} \pm 1.65 \times 10^{-1}$
[b]EC (m/z 36)	$1.74 \times 10^{-5} \pm 3.21 \times 10^{-6}$	$2.12 \times 10^{-1} \pm 3.18 \times 10^{-2}$

[a] [GPIC]= $\alpha \cdot V_S + \beta$.
[b] [Sunset OCEC]= $\alpha \cdot V_S + \beta$.

ACPD
11, 1219–1264, 2011

Table 4. Major ion markers of the 10 major particle types in Harrow.

Cluster types	Major ions
OC-S	$^{18}NH_3^+$, $^{43}C_3H_7^+$, $^{97}HSO_4^-$
OC-S-N	$^{18}NH_3^+$, $^{43}C_3H_7^+$, $^{26}CN^-$, $^{46}NO_2^-$, $^{62}NO_3^-$, $^{97}HSO_4^-$
OC	$^{27}C_2H_3^+$, $^{39}K^+$, $^{43}C_3H_7^+$, $^{97}HSO_4^-$
EC-OC	$^{12}C_2^+$, $^{36}C_3^+$, $^{97}HSO_4^-$
Amines	$^{59}C_3H_9N^+$
Fireworks	$^{39}K^+$, $^{154}BaOH+$, $^{46}NO_2^-$, $^{62}NO_3^-$, $^{163}K(NO_3)_2^-$, $^{125}H(NO_3)_2^-$
EC (I)	$^{12n}C_n^\pm$, $^{23}Na^+$
EC (II)	$^{12n}C_n^\pm$, $^{39}K^+$, $^{46}NO_2^-$, $^{62}NO_3^-$, $^{97}HSO_4^-$
Dust	$^{23}Na^+$, $^{39}K^+$, $^{40}Ca^+$, $^{56}CaO^+$, $^{16}O^-$, $^{17}OH^-$, $^{46}NO_2^-$, $^{62}NO_3^-$
Dust-Na	$^{23}Na^+$, $^{16}O^-$, $^{17}OH^-$, $^{46}NO_2^-$, $^{62}NO_3^-$, $^{131}NaNO_2NO_3^-$

ACPD
11, 1219–1264, 2011

Table 5. Contribution (%) of the 10 particle types to $PM_{2.5}$ major chemical components in Harrow.

Cluster types	Sulphate	Nitrate	Ammonium	OM[a]	EC
OC-S	33.4	20.9	35.5	30.9	14.5
OC-S-N	29.2	33.5	24.1	29.5	15.2
OC	15.0	15.4	11.4	18.9	7.9
EC-OC	16.2	10.0	10.9	6.4	42.5
Amines	3.4	7.0	11.0	8.0	3.2
Fireworks	0.1	2.2	0.2	0.4	0.2
EC (I)	0.9	0.3	4.9	1.5	12.8
EC (II)	0.7	1.1	0.6	0.7	2.7
Dust	1.1	8.7	1.4	3.7	1.0
Dust-Na	0.0	0.9	0.0	0.0	0.0

[a] OM=1.4 × OC.

ACPD
11, 1219–1264, 2011

Fig. 1. Locations of monitoring sites during the SPORT (Toronto) and BAQS-Met (Harrow) campaigns.

ACPD
11, 1219–1264, 2011

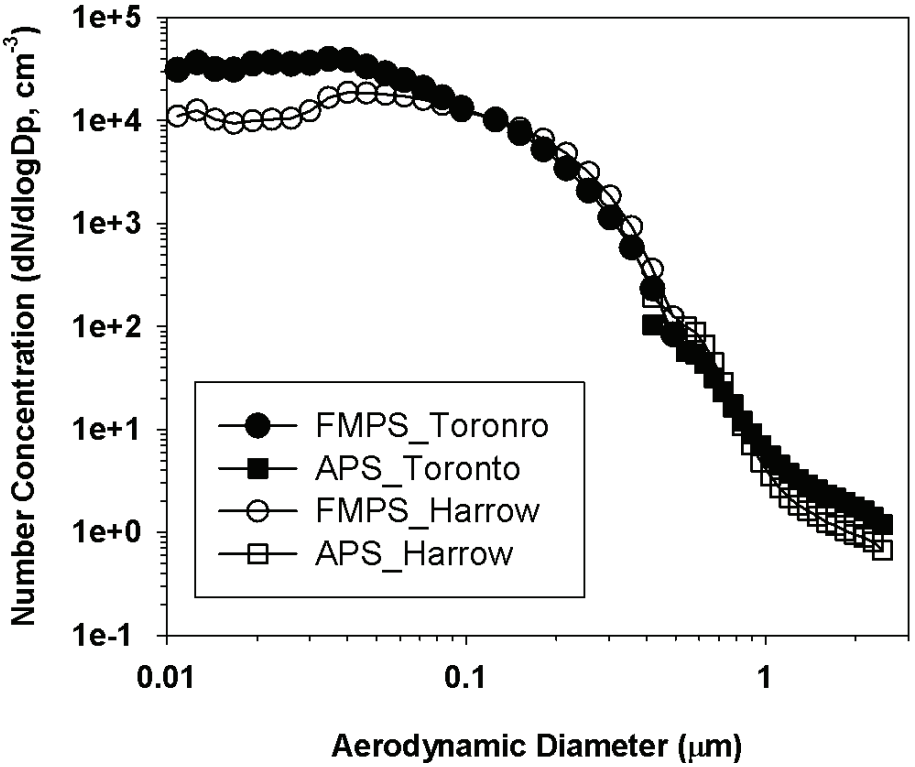

Fig. 2. Average size distributions of particles measured by the FMPS (0.01 μm–0.50 μm) and the APS (0.30 μm–2.50 μm) in Toronto and Harrow.

ACPD
11, 1219–1264, 2011

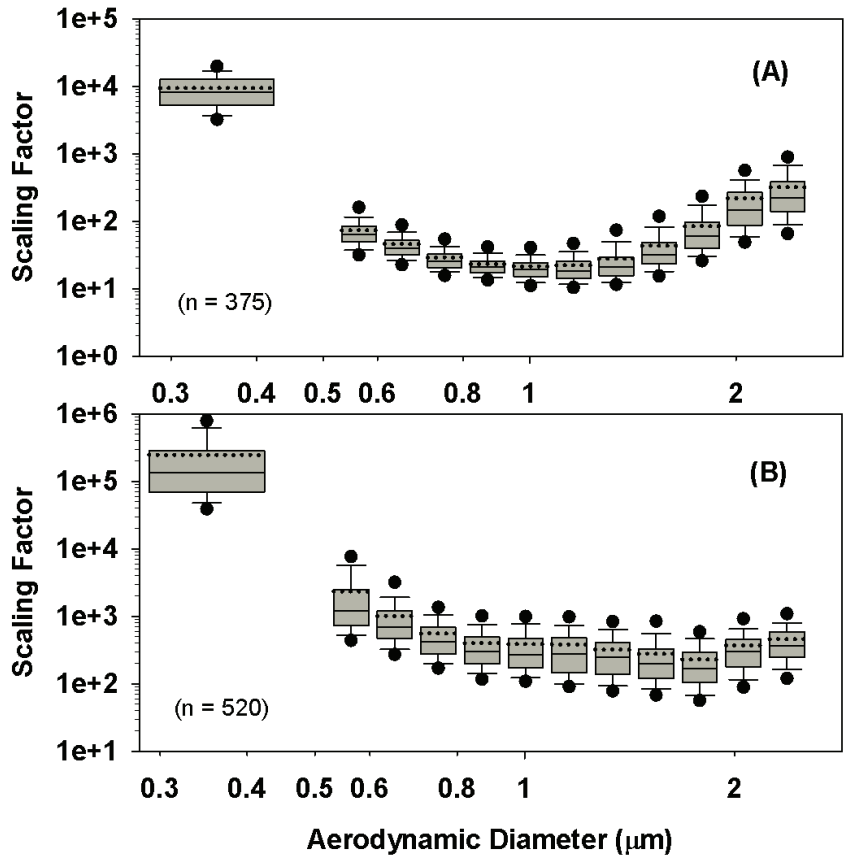

Fig. 3. ATOFMS scaling factor using APS (for d_a >0.52 μm) and FMPS (for 0.1< d_a <0.5 μm) for January–February 2007 in Toronto **(A)** and for June–July 2007 in Harrow **(B)**. *n*: number of hourly averages. Box-whisker plots demonstrate the median (solid line), mean (dotted line), quartile (box), 90% percentile (whiskers), and 95% percentile (dots).

ACPD
11, 1219–1264, 2011

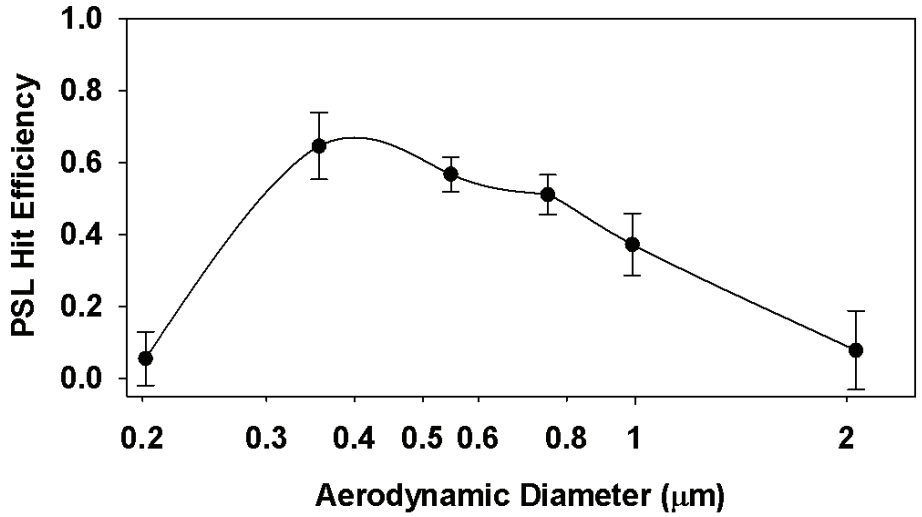

Fig. 4. Variability in ATOFMS hit efficiency as a function of PSL sizes. Error bars represent standard deviations.

ACPD
11, 1219–1264, 2011

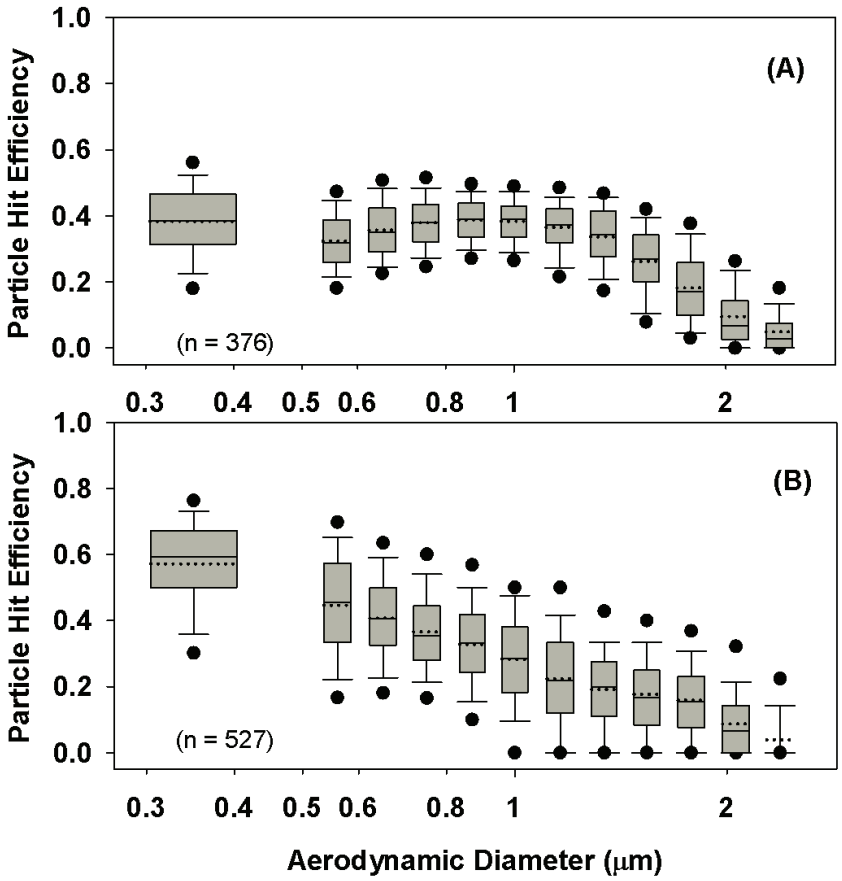

Fig. 5. ATOFMS hit efficiency of particles during the SPORT in Toronto **(A)** and the BAQS-Met in Harrow **(B)** campaigns in 2007. Box-whisker plots demonstrate the median (solid line), mean (dotted line), quartile (box), 90% percentile (whiskers), and 95% percentile (dots).

ACPD
11, 1219–1264, 2011

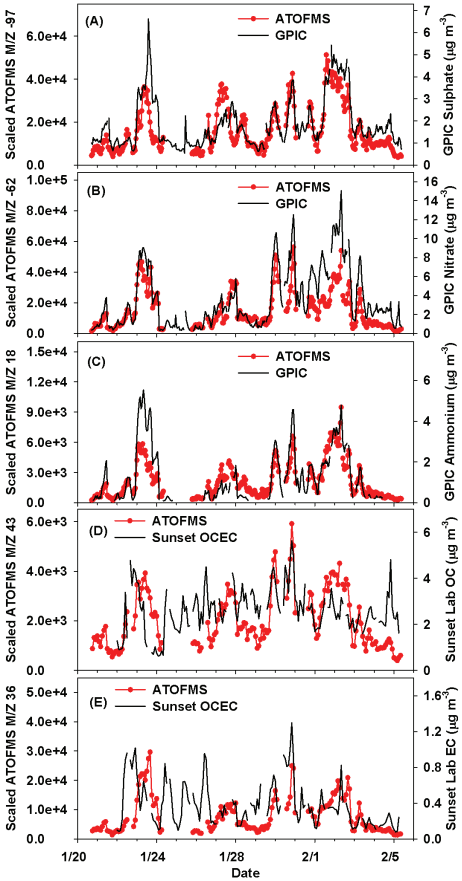

Fig. 6. Comparison between total ATOFMS relative peak area scaled by particle transmission efficiency and corresponding GPIC measurements as well as Sunset Lab OC and EC concentrations during the SPORT campaign in Toronto. **(A)** sulphate, **(B)** nitrate, **(C)** ammonium, **(D)** OC, and **(E)** EC.

ACPD
11, 1219–1264, 2011

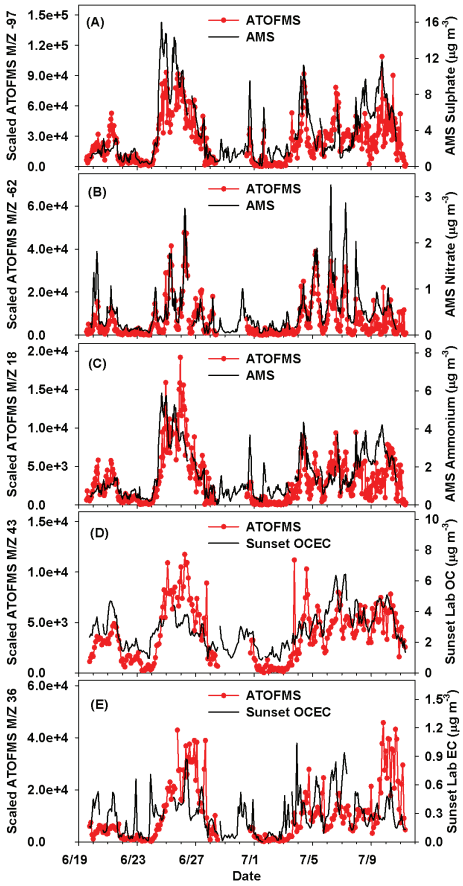

Fig. 7. Comparison between total ATOFMS relative peak area scaled by particle transmission efficiency and corresponding AMS measurements as well as Sunset Lab OC and EC concentrations during the BAQS-Met campaign in Harrow. **(A)** sulphate, **(B)** nitrate, **(C)** ammonium, **(D)** OC, and **(E)** EC.

ACPD
11, 1219–1264, 2011

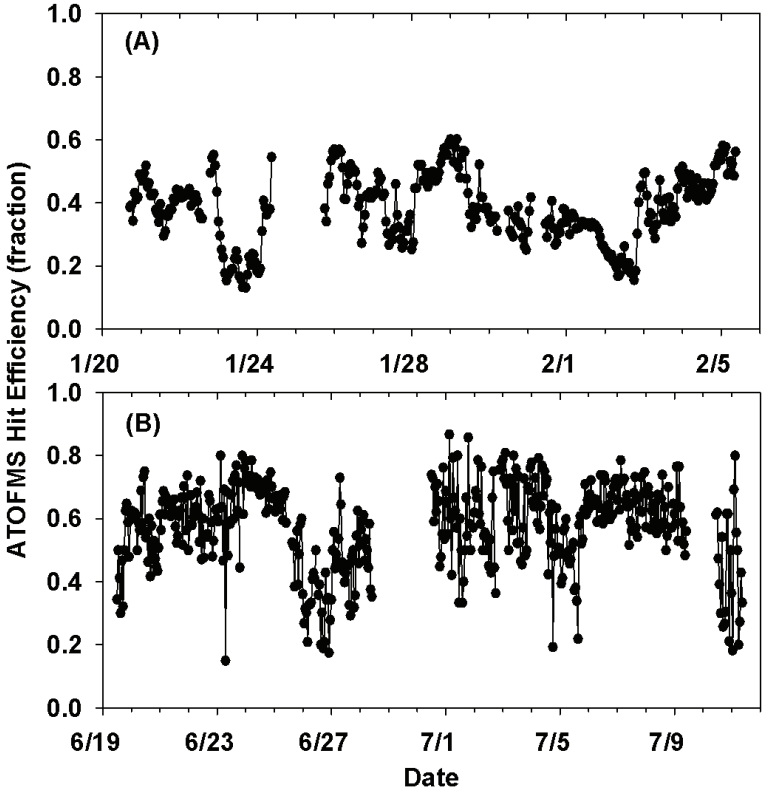

Fig. 8. ATOFMS hit efficiency for particle smaller than 0.52 µm in Toronto **(A)** and Harrow **(B)**.

ACPD
11, 1219–1264, 2011

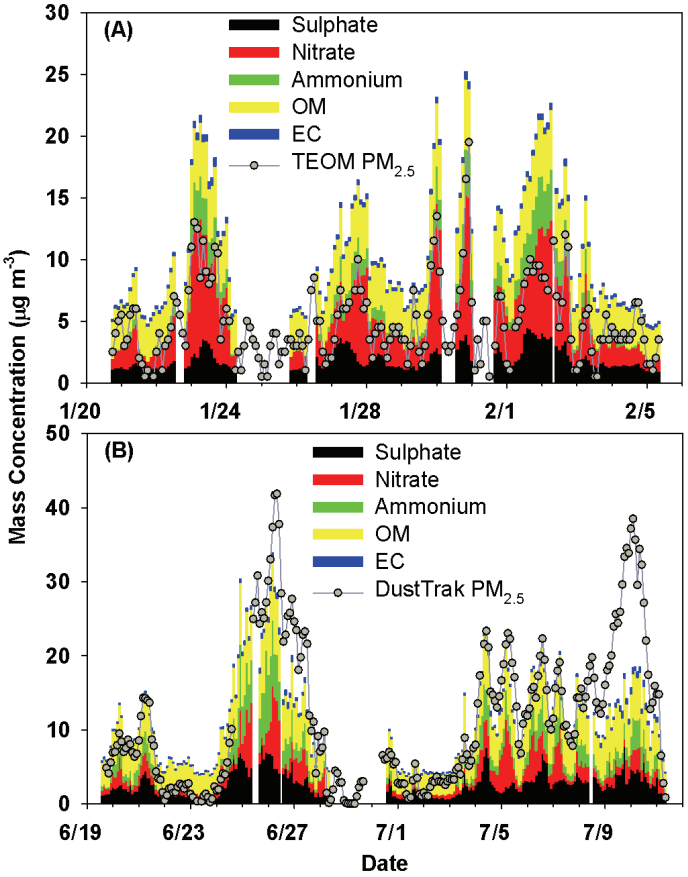

Fig. 9. Stacked two hour resolution chemical species calculated by using scaled ATOFMS RPA and measured $PM_{2.5}$ mass concentrations by the TEOM in Toronto **(A)** and the DustTrak in Harrow **(B)**.

ACPD
11, 1219–1264, 2011

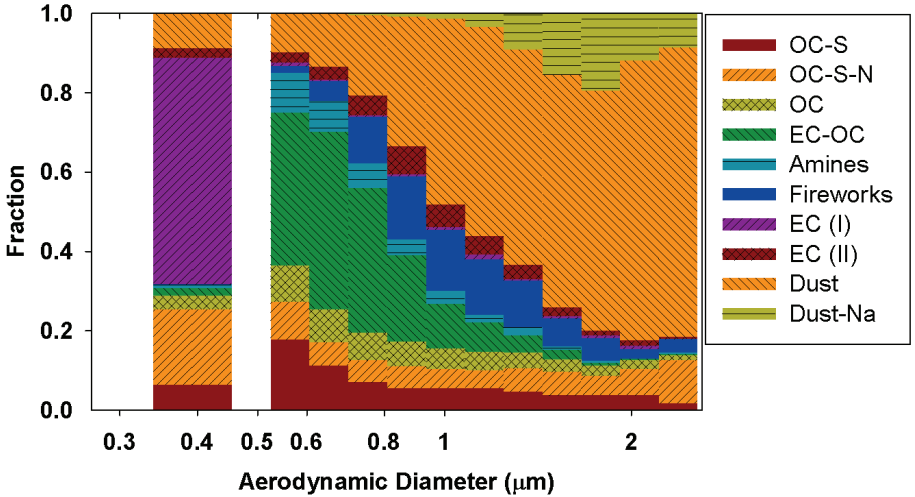

Fig. 10. The proportion of particles of each type, based on particle number, as a function of particle size.

ACPD
11, 1219–1264, 2011

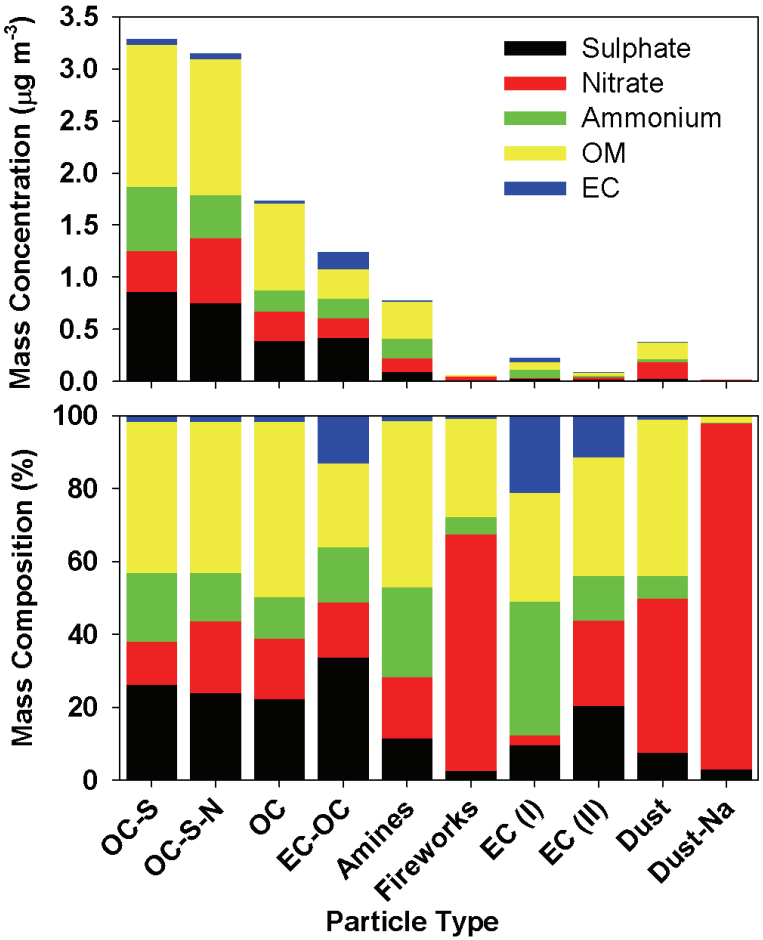

Fig. 11. Average mass concentration **(A)** and composition **(B)** of the five $PM_{2.5}$ chemical components in the 10 particle types.

ACPD
11, 1219–1264, 2011